ORIGINAL PAPER

Czesław Szymczak · Marcin Kujawa[ID]

Distortional buckling of composite thin-walled columns of a box-type cross section with diaphragms

Abstract Distortional buckling of axially compressed columns of box-like composite cross sections with and without internal diaphragms is investigated in the framework of one-dimensional theory. The channel members are composed of unidirectional fibre-reinforced laminate. Two approaches to the member orthotropic material are applied: homogenization based on the theory of mixture and periodicity cells, and homogenization based on the Voigt–Reuss hypothesis. The principle of stationary total potential energy is applied to derive the governing differential equation. The obtained buckling stress is valid in the linear elastic range of column material behaviour. Numerical examples address simply supported columns, and analytical critical stress formulas are derived. The analytical and FEM solutions are compared, and sufficient accuracy of the results is observed.

List of symbols

a	Height of cross section
f	Fibre volume fraction
n	Number of half-waves of a buckling mode
r_0	Polar radius of gyration
u	Displacement of cross section corner
v_{lt}	Homogenized Poisson's ratio
v_l	Poisson's ratio in the longitudinal direction
v_t	Poisson's ratio in the transverse direction
v_m	Poisson's ratio of the matrix
v_f	Poisson's ratio of fibres
x; y; z	Cartesian coordinate system
A	Area of cross section
D_l	Elastic modulus in the longitudinal direction
D_t	Elastic modulus in the transverse direction
E_l	Homogenized Young's modulus in the longitudinal direction
E_t	Homogenized Young's modulus in the transverse direction

C. Szymczak
Department of Structural Engineering, Faculty of Ocean Engineering and Ship Technology,
Gdańsk University of Technology, G. Narutowicza 11/12 13, 80-233 Gdańsk, Poland
E-mail: szymcze@pg.edu.pl

M. Kujawa (✉)
Department of Structural Mechanics, Faculty of Civil and Environmental Engineering,
Gdańsk University of Technology, G. Narutowicza 11/12 13, 80-233 Gdańsk, Poland
E-mail: mark@pg.edu.pl

E_{m}	Young's modulus of the matrix
E_{f}	Young's modulus of fibres
G	Homogenized shear modulus
G_{m}	Shear modulus of the matrix
G_{f}	Shear modulus of fibres
J_0	Polar moment of inertia
J_{g}	Moment of inertia of wall cross section in the longitudinal direction
J_{p}	Moment of inertia of wall cross section in the transverse direction
J_{s}	Free torsion moment of inertia of wall cross section
K_{s}	Torsional stiffness of cross section
K_{g}	Longitudinal stiffness of cross section
K_{γ}	Distortional stiffness of cross section
$\overline{K}_{\gamma}$	Diaphragm stiffness
L	Length of column
L_0	Characteristic length of column
M_{p}	Bending moment of walls in the transverse direction
M_{g}	Bending moment of walls in the longitudinal direction
P	Compressive axial load
P_{cr}	Critical distortional buckling load
U^{I}	Potential energy of compressive load due to bending
U^{II}	Potential energy of compressive load due to torsion
V	Elastic strain energy
V_{g}	Potential energy of elastic bending
V_{p}	Potential energy of cross-sectional distortion
V_{s}	Potential energy of torsion
γ	Distortion angle
δ	Wall thickness
η	Coefficient of characteristic length of column
σ_{b}	Buckling stress
σ_{cr}	Critical buckling stress
$\sigma_{\mathrm{cr,min}}$	Minimum critical buckling stress
Π	Total potential energy

1 Introduction

In structural engineering problems, one-dimensional classical theories are often applied to investigate mathematical models of columns, assuming non-deformable member cross sections [21,34,35,39,40]. Unfortunately, this assumption is not valid in many structural engineering areas, e.g. in stability analysis of thin-walled members without diaphragms. To date, many papers have addressed the stability of members, including distortion of the member cross section, and analytical and numerical models of classical rods, plates, shells and thin-walled structures are currently in their development phases [13,26–29,37,38]. A number of works refer to the generalized beam theory (GBT) [1,2,5,10,11,14,30,31] and the finite strip method (FSM) [6,7,16,23]. The works [3,24] show the cases in which both methods are similar. It should be noted that in the same cases, the GBT and the FSM can be more computationally efficient than the finite element method (FEM) [41]. However, it is still very rare to find papers that consider distortional stability loss using a closed-form analytical solution. The articles [8,22,32] address a distortional form of stability loss in a column composed of isotropic elastic material due to cross section deformation. The present article is motivated by the need to complement the adequate research in the field.

This paper addresses a particular form of stability loss of a column of a closed deformable square cross section composed of orthotropic composite materials (see Fig. 1). Only elastic distortional buckling analysis is considered here. The analytical and numerical models of the column are taken into account. The differential equation for the problem is derived by means of the stationary energy principle. The column is composed of unidirectional fibre-reinforced laminate [4,9,17–20,25,36]. Two approaches to orthotropic modelling of the member material are applied: homogenization based on the theory of mixtures [21] and periodicity cells and homogenization based on the Voigt–Reuss hypothesis [4].
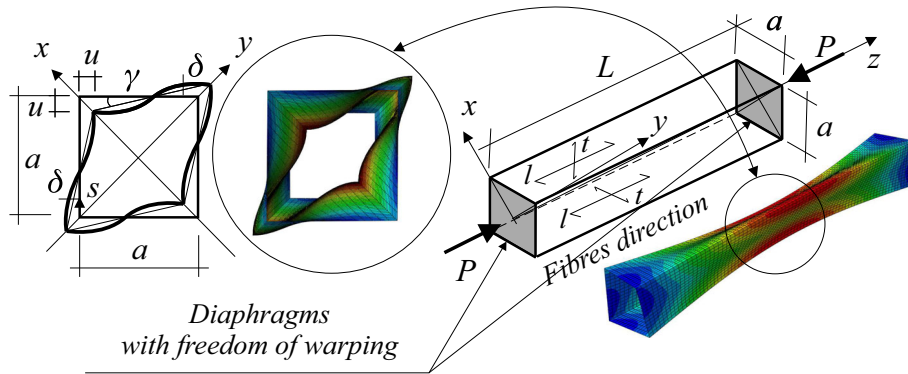
Fig. 1 Schematic diagram of the column and expected mode of distortional buckling

Numerical examples of simply supported axially compressed columns are presented. A comparative study of analytical and FEM results is also provided.

This paper continues the previous research described in [22,32,33]. At present, this research is focused on solving the problem posed in [22,32], assuming that the column is made of unidirectional fibre-reinforced laminate [33] with regard to plane stress. Furthermore, in developing the theoretical description, attention is paid to the influence of internal diaphragms on the stability of columns.

2 Elastic energy of distortional buckling

The major concern of this work is the distortional stability of an axially compressed composite thin-walled column with a box quadratic cross section stiffened by two diaphragms, where both ends are free to warp (see Fig. 1). The differential equation for the problem is derived by means of the stationary potential energy principle [35]. The total potential energy Π is the sum of the elastic strain energy V in the deformed walls of the column and the energy U of the axial loads. Two simplified homogenization methods for modelling the material are applied as follows: the first is related to the theory of mixture and periodicity cells (A) [21], and the second is based on the Voigt–Reuss hypothesis (B) [4]. The homogeneous orthotropic material for composite plates based on the theory of mixture and periodicity cells (A) [21] leads to the following formulas:

$$E_l = E_m(1 - f) + E_f f,$$
$$E_t = E_m \frac{E_m \left(1 - \sqrt{f}\right) + E_f \sqrt{f}}{E_m[1 - \sqrt{f} \left(1 - \sqrt{f}\right)] + E_f \sqrt{f} \left(1 - \sqrt{f}\right)},$$
$$G = G_m \frac{G_m \sqrt{f} \left(1 - \sqrt{f}\right) + G_f[1 - \sqrt{f} \left(1 - \sqrt{f}\right)]}{G_m \sqrt{f} + G_f \left(1 - \sqrt{f}\right)},$$
$$v_{lt} = v_m \left(1 - \sqrt{f}\right) + v_f \sqrt{f},$$
$$E_l v_{tl} = E_t v_{lt}, \tag{1}$$

where E_l and E_t are the homogenized Young's moduli for composite materials in the longitudinal and transverse directions, respectively, E_m and E_f are the Young's moduli for the matrix and fibres, respectively, G is the homogenized shear modulus, G_m and G_f are the shear moduli for the matrix and fibres, respectively, v_m and v_f are the Poisson's ratios for the matrix and fibres, respectively, f is the fibre volume fraction, and v_l and v_t are the homogenized Poisson's ratios in the longitudinal and transverse directions, respectively.

The second homogenization method based on the Voigt–Reuss hypothesis (B) [4] leads to the following:

$$E_l = E_m(1 - f) + E_f f,$$
$$E_t = \frac{E_f E_m}{E_f - E_f f + E_m f},$$
$$G = \frac{G_f G_m}{G_f - G_f f + G_m f},$$

$$v_{lt} = v_m(1 - f) + v_f f,$$
$$E_l v_{tl} = E_t v_{lt}. \tag{2}$$

Due to plane stress, the Young's moduli of elasticity in both directions should be modified to the elastic moduli in the longitudinal and transverse directions,

$$D_l = \frac{E_l}{1 - v_{lt} v_{tl}} = E_l \frac{1}{1 - \frac{E_t}{E_l} v_{lt}^2},$$

$$D_t = E_t \frac{1}{1 - \frac{E_t}{E_l} v_{lt}^2}. \tag{3}$$

2.1 The potential energy of cross-sectional distortion

The pattern of element cross-sectional distortion is shown in Fig. 1 and is defined by the distortional angle γ. The potential energy of the cross-sectional distortions V_p due to wall bending in the transverse direction is expressed by

$$V_p = \frac{1}{2} 4 \int_0^L \int_0^a \frac{M_p^2(s, z)}{D_t J_p} ds dz = \frac{24 D_t J_p}{a} \int_0^L \gamma^2 dz = \frac{1}{2} K_\gamma \int_0^L \gamma^2 dz, \tag{4}$$

where $M_p(s, z) = M_p(z)\left(\frac{2s}{a} - 1\right)$ and $M_p(z) = M_p = \frac{6D_t J_p}{a^2} 2u = 6D_t J_p \frac{\gamma}{a}$ is the bending moment of the wall in the transverse direction as shown in Fig. 17a of Appendix A (variable s is shown in Fig. 1), D_t is the elastic modulus of the wall material in the transverse direction, $J_p = \frac{\delta^3}{12}$ is the moment of inertia of the wall cross section in the transverse direction, a is the height of the cross section, and the distortional stiffness K_γ is defined as

$$K_\gamma \overset{\text{def}}{=} \frac{48 D_t J_p}{a} = \frac{4 D_t}{a} \delta^3, \tag{5}$$

where δ is the wall thickness.

2.2 Bending potential energy of the column in the longitudinal direction

The elastic potential energy V_g of the column in the longitudinal direction is (see Fig. 17b of Appendix A)

$$V_g = \frac{1}{2} 4 \int_0^L \frac{M_g^2}{D_l J_g} dz = \frac{1}{2} K_g \int_0^L \gamma''^2 dz, \tag{6}$$

where $M_g = -D_l J_g u'' = -D_l J_g \frac{a}{2} \gamma''$ is the bending moment of the walls in the longitudinal direction, $J_g = \frac{\delta a^3}{12}$ is the moment of inertia of the wall cross section in the longitudinal direction, D_l is the elastic modulus of the wall material in the longitudinal direction, and the longitudinal stiffness K_g is defined as

$$K_g \overset{\text{def}}{=} D_l J_g a^2 = \frac{D_l a^5}{12} \delta. \tag{7}$$

2.3 Potential energy of torsion of the cross section walls

Furthermore, the energy of torsion of the cross section walls V_s is taken into account (see Appendix A):

$$V_s = \frac{1}{2} 4 G J_s \int_0^L \gamma'^2 dz = \frac{2}{3} G \delta^3 a \int_0^L \gamma'^2 dz = \frac{1}{2} K_s \int_0^L \gamma'^2 dz, \tag{8}$$

where G is the shear modulus, $J_s = \frac{1}{3} a \delta^3$ is the free torsion moment of inertia of the wall, and the torsional stiffness K_s is defined as

$$K_s \overset{\text{def}}{=} \frac{4}{3} G a \delta^3. \tag{9}$$

2.4 Potential energy of end loads

It is supposed that the axial load P is uniformly distributed over the column cross section at both ends (see Figs. 17a, c of Appendix A). Hence, the total energy is the sum of the energy due to bending and the energy due to torsion of the walls. The first term corresponding to bending is

$$U^I = -\frac{1}{2}4\frac{P}{4}\int_0^L u'^2 dz = -\frac{1}{2}P\left(\frac{a}{2}\right)^2 \int_0^L \gamma'^2 dz = -\frac{1}{8}Pa^2 \int_0^L \gamma'^2 dz, \tag{10}$$

where $u = \gamma\frac{a}{2}$ is the displacement of the cross section corner (see Fig. 1 and Fig. 17a of Appendix A).

The second potential energy part U^{II} is related to the torsion and is the sum of the energy of the walls,

$$U^{II} = -\frac{1}{2}4\frac{P}{4}r_0^2 \int_0^L \gamma'^2 dz = -\frac{1}{2}Pr_0^2 \int_0^L \gamma'^2 dz, \tag{11}$$

where r_0^2 is the square of the polar radius of gyration of a single wall and is given by

$$r_0^2 = \frac{J_0}{A} = \frac{\frac{1}{12}(a^3\delta + \delta^3 a)}{a\delta} = \frac{1}{12}(a^2 + \delta^2), \tag{12}$$

where J_0 is the polar moment of inertia and A is the wall cross-sectional area.

2.5 Total potential energy

The total potential energy Π is the sum of the energy parts as follows:

$$\Pi = V_p + V_g + V_s + U^I + U^{II}. \tag{13}$$

Considering the individual components, we obtain

$$\Pi = \frac{1}{2}K_\gamma \int_0^L \gamma^2 dz + \frac{1}{2}\left(K_s - \frac{1}{4}Pa^2 - Pr_0^2\right)\int_0^L \gamma'^2 dz + \frac{1}{2}K_g \int_0^L \gamma''^2 dz. \tag{14}$$

A necessary condition for stationary total potential energy (14) leads to the differential equation [32]

$$K_g\gamma^{IV} + \left\{\frac{Pa^2}{12}\left[4 + \left(\frac{\delta}{a}\right)^2\right] - K_s\right\}\gamma'' + K_\gamma\gamma = 0. \tag{15}$$

Equation (15) can be rewritten as

$$\gamma^{IV} + 2\alpha\gamma'' + \beta^2\gamma = 0, \tag{16}$$

where

$$2\alpha = \frac{1}{K_g}\left\{\frac{Pa^2}{12}\left[4 + \left(\frac{\delta}{a}\right)^2\right] - K_s\right\} = \frac{P(4a^2 + \delta^2) - 16aG\delta^3}{a^5\delta D_l} \tag{17}$$

and

$$\beta^2 = \frac{K_\gamma}{K_g} = 48\frac{D_t\delta^2}{D_l a^6}. \tag{18}$$

The general solution of Eq. (16) is

$$\gamma(z) = C_1 \sin(t_1 z) + C_2 \cos(t_1 z) + C_3 \sin(t_2 z) + C_4 \cos(t_2 z), \tag{19}$$

where t_1 and t_2 are

$$t_1 = \sqrt{\alpha - \sqrt{\alpha^2 - \beta^2}}, \quad t_2 = \sqrt{\alpha + \sqrt{\alpha^2 - \beta^2}}.$$

The constants C_1, C_2, C_3 and C_4 should be determined by means of the corresponding boundary conditions.

3 Buckling of a simply supported column

Let us consider a simply supported column of length L compressed by axial end loads P (see Fig. 1).

Substituting the boundary conditions

$$z = 0, \quad \gamma = 0, \quad \gamma'' = 0,$$
$$z = L, \quad \gamma = 0, \quad \gamma'' = 0$$

into Eq. (19), we arrive at the system of linear algebraic equations

$$
\begin{aligned}
C_2 + C_4 &= 0, \\
-C_2 t_1^2 - C_4 t_2^2 &= 0, \\
C_1 \sin(t_1 L) + C_3 \sin(t_2 L) &= 0, \\
-C_1 t_1^2 \sin(t_1 L) - C_3 t_2^2 \sin(t_2 L) &= 0.
\end{aligned}
\tag{20}
$$

The system's solution is

$$t_2^2 L^2 = n^2 \pi^2, \tag{21}$$

where n is the number of half-waves of a buckling mode.

A number of operations results in

$$2\alpha = \frac{n^2 \pi^2}{L^2} + \beta^2 \frac{L^2}{n^2 \pi^2}. \tag{22}$$

Subsequently, the buckling load P_b^n corresponding to the number of buckling mode half-waves n is derived,

$$P_b^n = \frac{\pi^2 a^5 D_l n^2 \delta}{L^2 (4a^2 + \delta^2)} + \frac{48 \delta^3 D_t L^2}{\pi^2 n^2 a (4a^2 + \delta^2)} + \frac{16 a G \delta^3}{4a^2 + \delta^2}. \tag{23}$$

Next, the buckling stress is expressed in terms of $m = \frac{n\pi}{L}$,

$$\sigma_b = m^2 \frac{a^4 D_l}{4(4a^2 + \delta^2)} + \frac{1}{m^2} \frac{12 \delta^2 D_t}{a^2 (4a^2 + \delta^2)} + \frac{4 \delta^2 G}{4a^2 + \delta^2}. \tag{24}$$

The critical buckling stress σ_{cr} is assumed to be the minimum buckling stress with respect to the integer number of buckling half-waves n. To find the minimum stress, we incorporate its relation with the relative length of the column shown in Fig. 2. Applying the graph shown in Fig. 2, it is possible to find the number of half-waves of a buckling mode n corresponding to the critical buckling stress σ_{cr}.

The minimum critical buckling load results from the first derivative of the buckling load (24) with respect to m,

$$\frac{\mathrm{d}\sigma_b}{\mathrm{d}m} = 0, \tag{25}$$

which leads to the column length corresponding to the minimum critical stress (note that L is usually known, so the characteristic length L_0 and number of half-waves n are investigated)

$$L = \eta L_0, \tag{26}$$

where L_0 is equal to

$$L_0 = \frac{1}{2} \pi a \sqrt[4]{\frac{1}{3} \frac{D_l}{D_t} \left(\frac{a}{\delta}\right)^2}. \tag{27}$$

Substituting results (25) into formula (24), it is possible to find the minimum critical buckling stress

$$\sigma_{cr,min} = \frac{2\delta \left(a \sqrt{3 D_l D_t} + 2\delta G\right)}{4a^2 + \delta^2}. \tag{28}$$

The buckling critical stress versus member length relation, scaled by the characteristic length L_0, is illustrated in Fig. 2.

To determine the critical buckling load P_{cr} or stress σ_{cr}, it is first necessary to find the characteristic length coefficient of the column η (26); next, the number of half-waves n is taken from Fig. 2. Substituting the number of half-waves n into (24), the critical buckling stress is obtained.
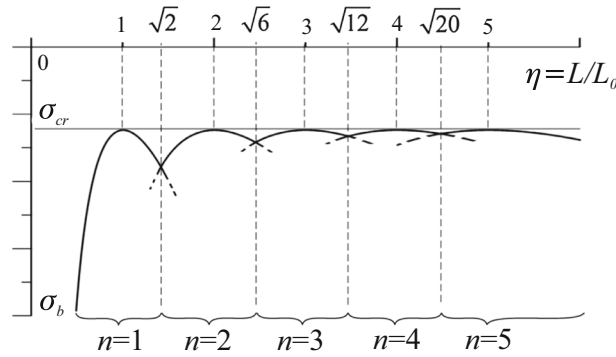
Fig. 2 Critical buckling stress versus ratio of the member length to its characteristic value
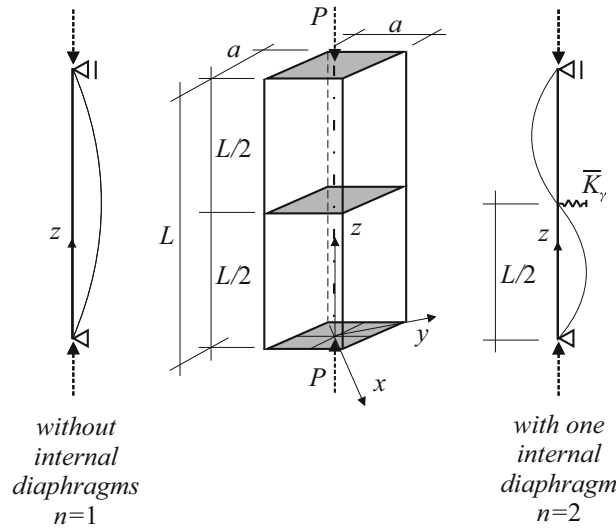

Fig. 3 Column with an additional internal diaphragm

4 Effect of diaphragm introduction

This paper studies the behaviour of thin-walled columns with closed square cross sections with two supports/diaphragms on freely warping column ends. In practice, to increase the critical load, additional internal diaphragms may be added (see Fig. 3). The best locations of diaphragms are in the cross sections in the middle of each half-wave where the mode amplitude occurs. For the appropriate diaphragm stiffness, the number of the half-waves increases twofold, increasing the critical stresses.

We first examine the case of a single half-wave as a buckling mode. The analysis is focused on the minimum stiffness of the internal diaphragm located in the column middle $\overline{K}_\gamma$ needed to double the number of half-waves (see Fig. 17d of Appendix A). The effect of such a diaphragm is equivalent to a rigid support; thus, no distortion occurs here, and eventually, the critical buckling stress (24) increases.

The solution of (16) satisfies the boundary conditions formulated due to the column part from the left support to the internal diaphragm:

$$
\begin{aligned}
z &= 0, \quad \gamma = 0, \\
z &= 0, \quad \gamma'' = 0, \\
z &= L/2, \quad \gamma' = 0.
\end{aligned}
\tag{29}
$$

The first two boundary conditions represent the simply supported end; third condition expresses symmetry of distortion along the column axis. The solution satisfying these three boundary conditions (29) reads

$$
\gamma(z) = C_1 \left[\sin(t_1 z) - \frac{t_1 \cos(\rho_1)}{t_2 \cos(\rho_2)} \sin(t_2 z) \right],
\tag{30}
$$

Table 1 Material properties for fibres and the matrix

	Glass fibres	Epoxy matrix
Density (kg/m^3)	2450	1246
Young's modulus (GPa)	71	3.5
Kirchhoff's modulus (GPa)	30	1.25
Poisson's ratio (–)	0.22	0.33

where $\rho_1 = \frac{1}{2}t_1 L$, $\rho_2 = \frac{1}{2}t_2 L$.

Moreover, we have the fourth condition in the diaphragm location

$$z = L/2, \quad K_g \gamma''' = \frac{1}{2}\overline{K}_\gamma \gamma. \tag{31}$$

Substitution of Eqs. (30) into (31) leads to the diaphragm stiffness formula

$$\overline{K}_\gamma = 4K_g \frac{t_1 \sqrt{\alpha^2 - \beta^2} \cos(\rho_1)}{\sin(\rho_1) - \frac{t_1 \cos(\rho_1)}{t_2 \cos(\rho_2)} \sin(\rho_2)}. \tag{32}$$

Equation (32) represents the relation between the critical load P_{cr} and the diaphragm stiffness, if for example its value reaches zero then

$$\cos(\rho_1) = 0 \rightarrow \rho_1 = \frac{1}{2}t_1 L = \frac{1}{2}\pi n, \tag{33}$$

and the critical buckling load of the column without the internal diaphragm is stated by (23).

In order to find the diaphragm stiffness corresponding to a higher buckling mode $n = 2$, it is necessary to determine the coefficients α, t_1, t_2 [see Eqs. (17), (18) and (19)] due to the critical load related to this higher mode.

It should be emphasized that the additional diaphragm introduced in the middle cross section leads to higher critical stresses, while the ratio of the column length to its characteristic length η is less then $\sqrt{2} \approx 1.41$ (see Fig. 2).

When the number of half-waves n in the buckling mode is higher, all half-wave sections should be considered separately as simply supported columns of length L/n. Consequently, the n diaphragms should be situated in the middle cross sections of each half-wave.

5 Examples—analytical and numerical solutions

Consider an axially compressed thin-walled column of square cross section made of unidirectional fibre-reinforced composite material, as shown in Fig. 5. The material properties of the epoxy matrix and glass fibres are presented in Table 1.

The numerical and analytical solutions presented in this paper are related to the axially compressed simply supported column shown in Fig. 5.

Numerical analyses are carried out by means of ABAQUS software [15]. To estimate the critical buckling loads/stresses, a linear perturbation procedure (LBA) is applied. In the FEM analysis, due to the symmetry of the column cross section, only a quarter of each column was discretized, and the appropriate boundary conditions are presented in Fig. 5. To confirm the correctness of the assumed boundary conditions (see Figs. 4, 5) resulting from the symmetry of the static diagram, additional analysis of columns considering the entire cross-sectional geometry is carried out. Identical solutions are obtained in both cases with and without consideration of symmetry in the numerical models. The columns are modelled by finite membrane-strain shell elements with reduced integration type—S4R (0.02 × 0.02 m^2), i.e. 40 elements along the full cross section. The total number of finite elements in all cases is equal to 8000 for $L = 4$ m. The material behaviour is modelled by a linearly elastic orthotropic lamina-type procedure available in ABAQUS [15]. The parameters of material model types (A) and (B) ($E_1 = E_l$, $E_2 = E_t$, $v_{12} = v_{lt}$, $G_{12} = G_{13} = G_{23} = G$ and $v_{21} = (E_2/E_1)v_{12}$) are determined by Eqs. (1) and (2). The values of material parameters are shown in Table 2. The diaphragms in the
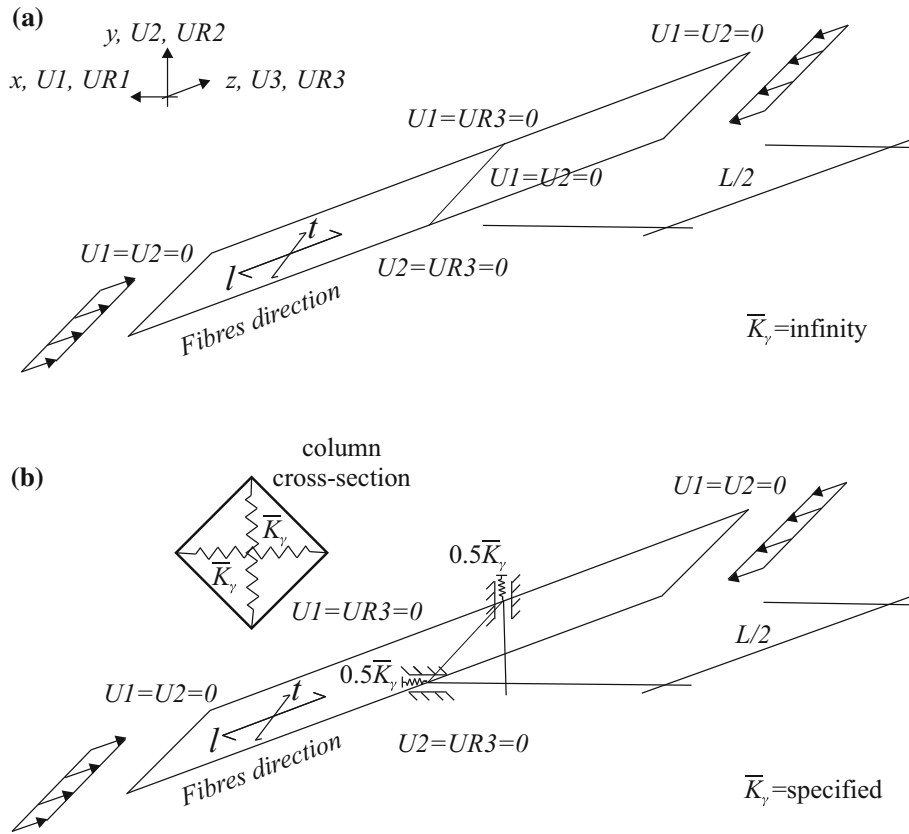
Fig. 4 Idea of supports (diaphragms) for one internal diaphragm—$n = 2$, assuming a infinite stiffness of the diaphragm and b a specified stiffness of the diaphragm
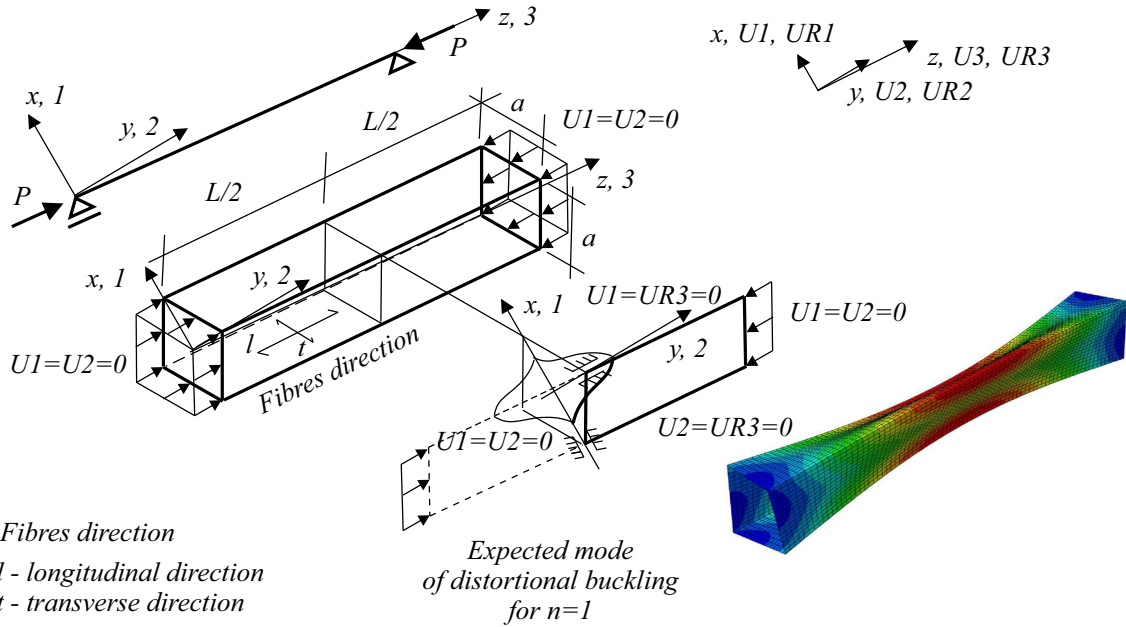

Fig. 5 Schematic FEM model, load, imposed boundary conditions and fibre direction (without symmetry and considering symmetry)

Table 2 Material parameters at different fibre volume fractions f for two types of homogenization (A) and (B)

f	Material's homogenization type	Material's homogenization type	Material's homogenization type	Material's homogenization type
	(A)(B)	(A) (B)	(A) (B)	(A) (B)
	E_l (GPa)	E_t (GPa)	G (GPa)	v_{lt} (−)
0.2	17.000	5.8414.322	1.6691.546	0.2810.308
0.4	30.500	8.4245.648	2.4662.027	0.2600.286
0.6	44.000	12.7748.148	4.0392.941	0.2450.264
0.8	57.500	22.64214.618	7.9595.357	0.2320.242
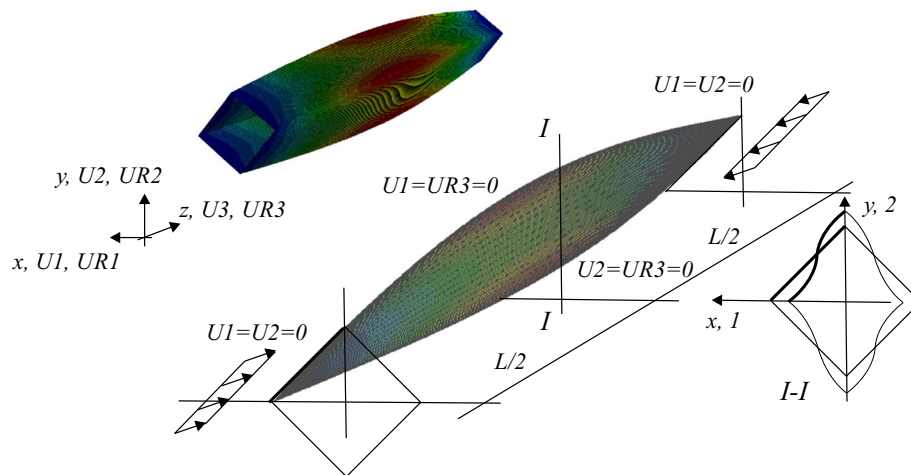
Fig. 6 Buckling mode at $n = 1$ for the full geometry of the column cross section and, based on symmetry, a quarter of the column cross section ($L = 4$ m, $a = 0.2$ m, $\delta = 0.001$ m)

Table 3 Critical buckling stresses and numbers of half-waves n for material model types (A) and (B) at different fibre volume fractions f

Glass–epoxy, $L = 4$ m, $a = 0.2$ m, $\delta = 0.001$ m

f	$\sigma_{cr,min}$		n		Critical buckling stress σ_{cr} (MPa)					
	(A)	(B)	Analyt.	FEM	Analy.	FEM	Diff. (%)	Analy.	FEM	Diff. (%)
			(A) and (B)		(A)			(B)		
0.2	44.4	38.1	1	1	45.2	39.4	13	40.4	35.0	13
0.4	70.8	57.8	1	1	74.1	64.4	13	65.2	56.3	14
0.6	104.6	83.1	1	1	108.7	94.8	13	93.9	81.1	14
0.8	159.8	127.6	1	1	161.1	141.5	12	135.6	118.0	13

Table 4 Critical buckling stresses and number of half-waves n—additional numerical examples

$L = 6$ m, $a = 0.25$ m, $\delta = 2$ mm

Material type	$\sigma_{cr,min}$ Analyt. (MPa)	No. of half-wave n		Critical buckling stress (MPa)				
		Analyt.	FEM	Analyt.		FEM	Diff. (%)	
			LBA	$\psi = 1$	$\psi = 0.9$	LBA	$\psi = 1$	$\psi = 0.9$
Boron–epoxy	461.44	1	1	461.64	415.48	403.19	13	3
Graphite–epoxy	223.39	1	1	278.29	250.46	225.36	19	10
Aramid–epoxy	142.97	1	1	144.36	129.92	124.73	14	4

Table 5 Specified stiffness of diaphragms $\overline{K}_\gamma$ Eq. (32) for different fibre volume fractions f (glass–epoxy, material model type (A), $L = 4$ m, $a = 0.2$ m, $\delta = 0.001$ m)

Specified stiffness of diaphragms analytical solution—(32)				
f	0.2	0.4	0.6	0.8
$\overline{K}_\gamma$ (Nm)	943.3	1749.3	2498.6	3071.0

Table 6 Buckling stress for a column with one diaphragm ($n = 2$) at different fibre volume fractions $f = 0.2$ and 0.8 (glass–epoxy, material model type (A), $L = 4$ m, $a = 0.2$ m, $\delta = 0.001$ m)

Buckling stress for a column with a diaphragm numerical solution—FEM				
	$\overline{K}_\gamma = $ infinity		$\overline{K}_\gamma = $ specified	
f	0.2	0.8	0.2	0.8
σ_{cr} (MPa)	87.5	306.1	87.5	306.2

columns are modelled using a Spring/Dashpot type connection: points to ground (for "simplified" numerical models based on symmetry) or two points (for full geometry numerical models) [15] (see Figs. 4, 6).

The major analytical results are shown in Tables 3, 4, 5 and 6. Furthermore, Figs. 7, 8, 9, 10, 11, 12 and 13 show the relationships between the buckling stresses σ_{cr} and the column length L, cross-sectional height a and wall thickness δ for five half-waves of the buckling modes and the minimum critical stresses $\sigma_{cr,min}$ versus the cross-sectional height a and wall thickness δ. The graphical relations shown in Figs. 7, 8, 9, 10, 11, 12 and 13 refer only to the material model type (A), but the characteristics and graphical representations of functions for the material model type (B) exhibit only slight variations. The figures more accurately indicate the differences between the (A) and (B) material model type solutions. It should be noted that the minimum critical buckling stresses are affected only by the cross-sectional dimensions, i.e. the cross-sectional height a and wall thickness δ, and are independent of the column length L. The relationship between the buckling stresses and the fibre volume fraction f for material model types (A) and (B) is shown. As the fibre volume fraction ratio increases, the critical stresses also increase. Unfortunately, the critical stress is significantly affected by the material homogenization method. The results shown in Figs. 7, 8, 9, 10, 11, 12 and 13 are limited to the assumed buckling stress range of 1000 MPa due to the range of material elasticity [12,17].

Additionally, the minimum critical stresses at different values of the wall thickness, related to the fibre volume fraction f, for the different material homogenization techniques (A) and (B) are shown in Fig. 14. Furthermore, the characteristic member lengths L_0 related to the fibre volume fraction f for various material type and homogenization methods (A) and (B) are shown in Fig. 15.

Table 3 shows the critical buckling stresses obtained with the proposed closed-form formula (24) and FEM procedures, compared for selected examples. The comparison of the analytical and FEM-based solutions indicates that the proposed closed-form analytical solutions are correct and acceptable from an engineering point of view (deviations not greater than 10%). This difference seems relatively stable and independent of the numerical example (see Table 3). A correction factor, ψ, for the critical buckling stress is therefore proposed. The value of the correction factor ψ should be equal to 0.9. Discrepancies can occur between the results at the limits of the individual ranges of n (the number of half-waves of a buckling mode) or if η (the coefficient of the characteristic length of a column) is much smaller than 1 (see Fig. 2).
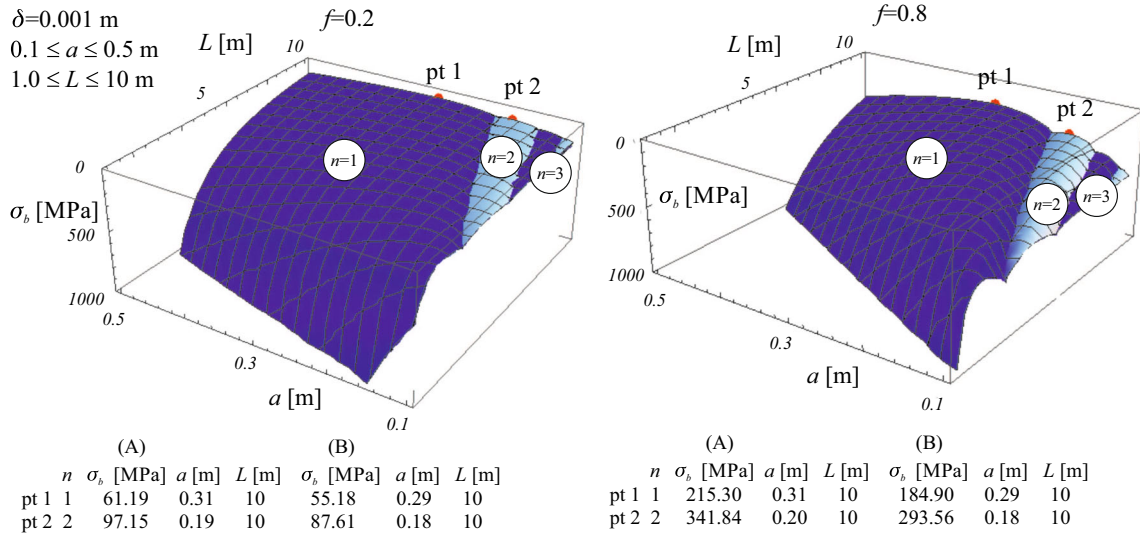
The proposed formula is confirmed by additional numerical analysis. Further examples are worked, assuming alternative geometric and material parameters as follows:

– geometric parameters: $L = 6$ m, $a = 0.25$ m, $\delta = 2$ mm,
– material parameters [17]: boron–epoxy—$E_l = 207$ GPa, $E_t = 21$ GPa, $G = 7$ GPa, $v_{lt} = 0.3$; graphite–epoxy—$E_l = 207$ GPa, $E_t = 5$ GPa, $G = 2.6$ GPa, $v_{lt} = 0.25$; aramid–epoxy—$E_l = 76$ GPa, $E_t = 5.5$ GPa, $G = 2.1$ GPa, $v_{lt} = 0.34$.

The buckling stresses and numbers of half-waves n are shown in Table 4.

Furthermore, axially compressed columns are analysed, including one with a single internal diaphragm (glass–epoxy, material model type (A), $L = 4$ m, $a = 0.2$ m, $\delta = 0.001$ m). Numerical analysis is carried out with the ABAQUS software. The numerical models are shown in Figs. 4 and 5.

Table 5 presents the stiffness of diaphragms for different fibre volume fractions, $f = 0.2, 0.4, 0.6, 0.8$, in the case of glass–epoxy material type (A) for the following geometric parameters of the column: $L = $

δ=0.001 m
$0.1 \leq a \leq 0.5$ m
$1.0 \leq L \leq 10$ m

	(A)			(B)		
n	σ_b [MPa]	a [m]	L [m]	σ_b [MPa]	a [m]	L [m]
pt 1 1	61.19	0.31	10	55.18	0.29	10
pt 2 2	97.15	0.19	10	87.61	0.18	10

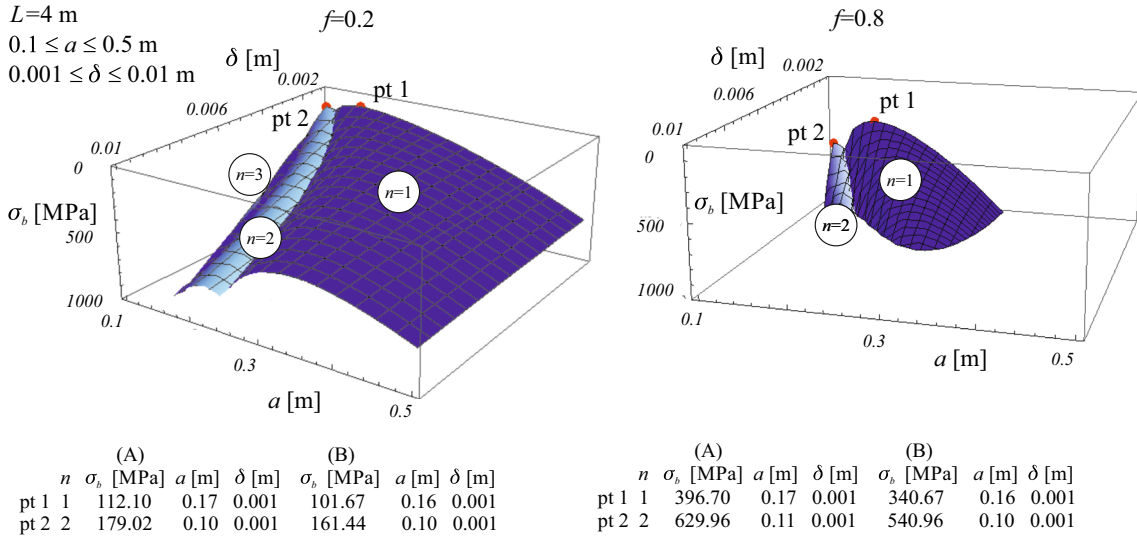|	(A)			(B)		
n	σ_b [MPa]	a [m]	L [m]	σ_b [MPa]	a [m]	L [m]
pt 1 1	215.30	0.31	10	184.90	0.29	10
pt 2 2	341.84	0.20	10	293.56	0.18	10

Fig. 7 Critical buckling stress σ_b versus cross-sectional height a and column length L for $f = 0.2$ and 0.8 (for $n = 1 - 5$, $\delta = 0.001$ m, material models (A) and (B))

δ=0.004 m
$0.1 \leq a \leq 0.5$ m
$1.0 \leq L \leq 10$ m

	(A)			(B)		
n	σ_b [MPa]	a [m]	L [m]	σ_b [MPa]	a [m]	L [m]
pt 1 1	154.26	0.49	10	139.11	0.46	10
pt 2 2	245.00	0.31	10	220.91	0.29	10

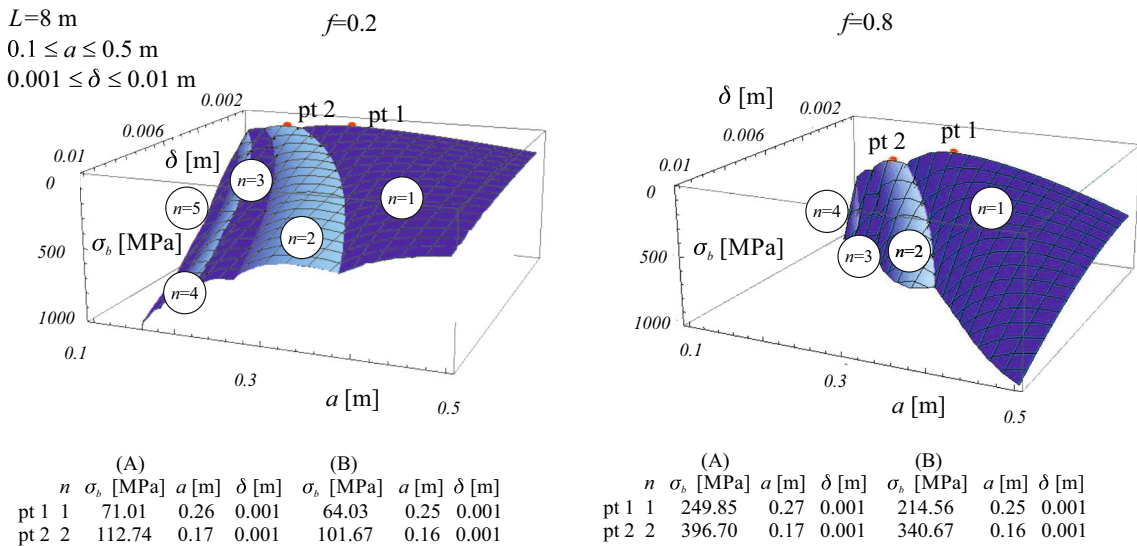|	(A)			(B)		
n	σ_b [MPa]	a [m]	L [m]	σ_b [MPa]	a [m]	L [m]
pt 1 1	542.81	0.50	10	466.13	0.46	10
pt 2 2	862.07	0.31	10	740.24	0.29	10
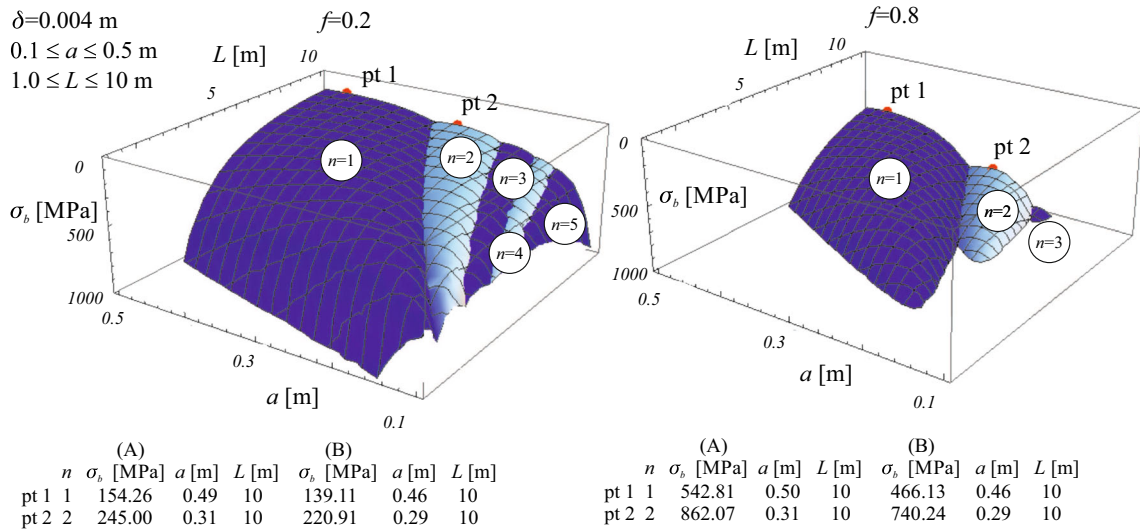
Fig. 8 Critical buckling stress σ_b versus cross-sectional height a and column length L for $f = 0.2$ and 0.8 (for $n = 1 - 5$, $\delta = 0.004$ m, material models (A) and (B))

4 m, $a = 0.2$ m, and $\delta = 0.001$ m. Table 6 shows the numerical results (FEM) for the buckling stresses of a column reinforced by one internal diaphragm in the middle of its length. It should be noted that the numerical results shown in Table 6 confirm the validity of the analytical formula (32) proposed to determine the stiffness of the diaphragm. Furthermore, as can be seen in the considered numerical examples (see the solutions in Tables 3 and 6), including an internal diaphragm in the column leads to increased critical stresses (by approximately 55%), particularly for the column at $f = 0.2$ from 39.4 MPa to 87.5 MPa and at $f = 0.8$ from 141.5 MPa to 306.1 MPa. The buckling modes of columns with internal diaphragms are shown in Fig. 16. The buckling modes presented in Fig. 16 correspond to both of the analysed cases, i.e. $\overline{K}_\gamma$ tends to infinity or is specified by formula (32).

	(A)			(B)				(A)			(B)		
n	σ_b [MPa]	a [m]	δ [m]	σ_b [MPa]	a [m]	δ [m]	n	σ_b [MPa]	a [m]	δ [m]	σ_b [MPa]	a [m]	δ [m]
pt 1 1	112.10	0.17	0.001	101.67	0.16	0.001	pt 1 1	396.70	0.17	0.001	340.67	0.16	0.001
pt 2 2	179.02	0.10	0.001	161.44	0.10	0.001	pt 2 2	629.96	0.11	0.001	540.96	0.10	0.001

Fig. 9 Critical buckling stress σ_b versus cross-sectional height a and wall thickness δ for $f = 0.2$ and 0.8 (for $n = 1 - 5$, $L = 4$ m, material models (A) and (B))

	(A)			(B)				(A)			(B)		
n	σ_b [MPa]	a [m]	δ [m]	σ_b [MPa]	a [m]	δ [m]	n	σ_b [MPa]	a [m]	δ [m]	σ_b [MPa]	a [m]	δ [m]
pt 1 1	71.01	0.26	0.001	64.03	0.25	0.001	pt 1 1	249.85	0.27	0.001	214.56	0.25	0.001
pt 2 2	112.74	0.17	0.001	101.67	0.16	0.001	pt 2 2	396.70	0.17	0.001	340.67	0.16	0.001

Fig. 10 Critical buckling stress, σ_b, versus cross-sectional height, a, and wall thickness, δ, for $f = 0.2$ and 0.8 (for $n = 1 - 5$, $L = 8$ m, material models (A) and (B))
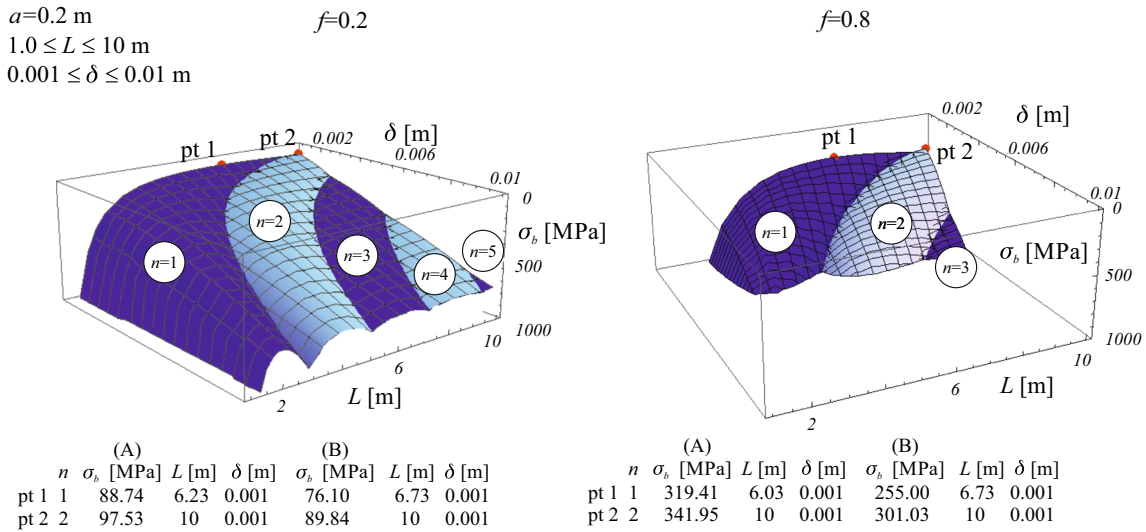
6 Discussion and conclusions

The issue of the distortional elastic stability of axially loaded thin-walled columns of box-type quadratic cross sections is discussed in this paper. The influence of internal diaphragms on the column stability is considered. Analytical closed formulas are derived for critical stresses and minimum buckling stresses independent of the number of the mode half-waves. The number of buckling mode half-waves can be determined by introducing the characteristic length of the column. Analytical characteristic length formulas are also provided. The results are compared with the FEM-based results obtained in the ABAQUS system [15].
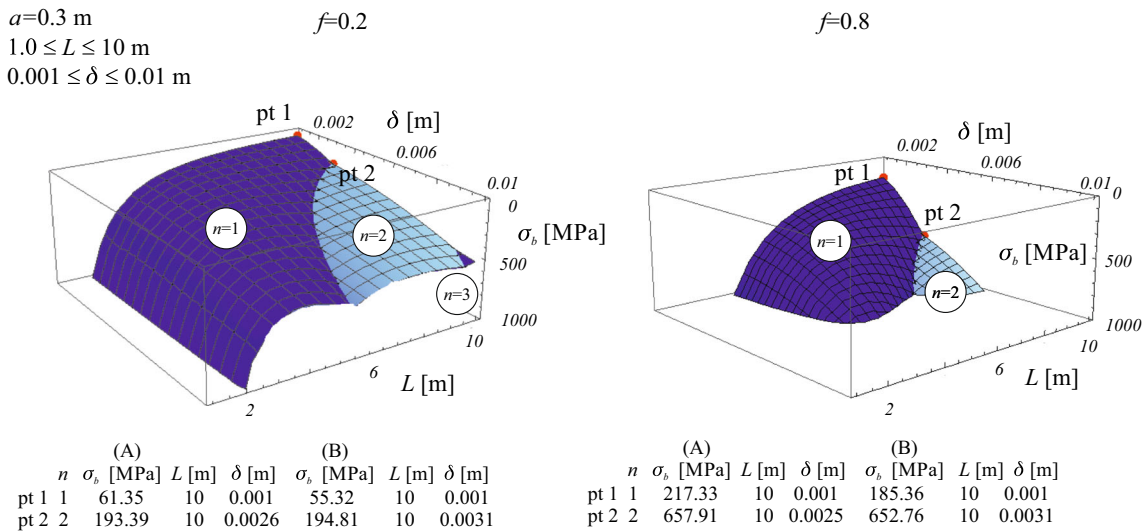
When the columns are composed of materials with a low modulus of elasticity, high elastic limit distortional buckling may occur in the elastic range, which is important in practical cases. Structural polymer composites/laminates (also considered in this paper) satisfy these conditions well (Fig. 17).

The simple formulas derived in the paper allow us to compute critical buckling loads, critical buckling stresses or minimal critical buckling stresses comparable to the FEM results with sufficient accuracy. Based

a=0.2 m
$1.0 \leq L \leq 10$ m
$0.001 \leq \delta \leq 0.01$ m

f=0.2

f=0.8

		(A)			(B)		
	n	σ_b [MPa]	L [m]	δ [m]	σ_b [MPa]	L [m]	δ [m]
pt 1	1	88.74	6.23	0.001	76.10	6.73	0.001
pt 2	2	97.53	10	0.001	89.84	10	0.001

		(A)			(B)		
	n	σ_b [MPa]	L [m]	δ [m]	σ_b [MPa]	L [m]	δ [m]
pt 1	1	319.41	6.03	0.001	255.00	6.73	0.001
pt 2	2	341.95	10	0.001	301.03	10	0.001

Fig. 11 Critical buckling stress σ_b versus column length L and wall thickness δ for $f = 0.2$ and 0.8 (for $n = 1 - 5$, $a = 0.2$ m, material models (A) and (B))
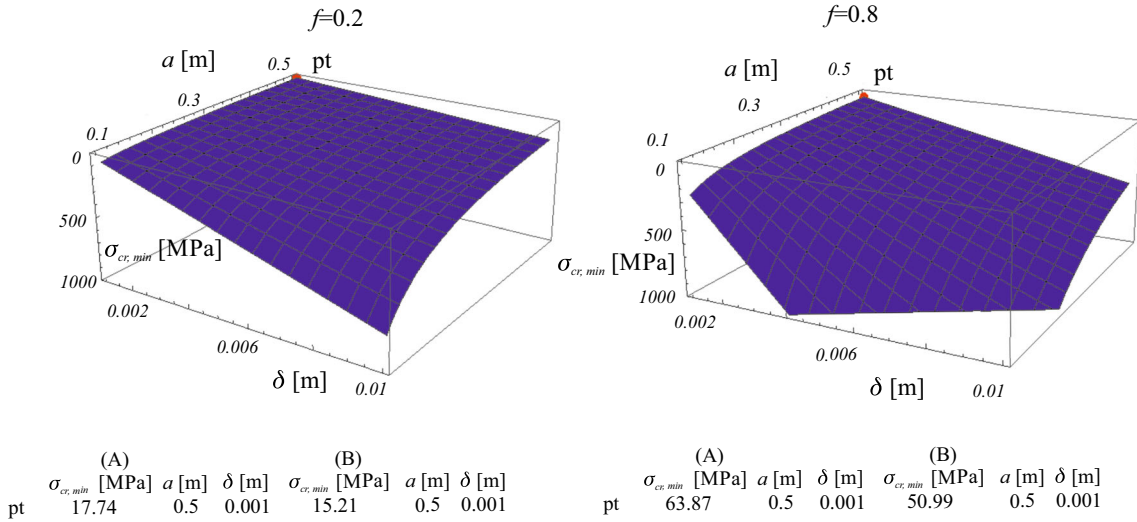
a=0.3 m
$1.0 \leq L \leq 10$ m
$0.001 \leq \delta \leq 0.01$ m

f=0.2

f=0.8

		(A)			(B)		
	n	σ_b [MPa]	L [m]	δ [m]	σ_b [MPa]	L [m]	δ [m]
pt 1	1	61.35	10	0.001	55.32	10	0.001
pt 2	2	193.39	10	0.0026	194.81	10	0.0031

		(A)			(B)		
	n	σ_b [MPa]	L [m]	δ [m]	σ_b [MPa]	L [m]	δ [m]
pt 1	1	217.33	10	0.001	185.36	10	0.001
pt 2	2	657.91	10	0.0025	652.76	10	0.0031

Fig. 12 Critical buckling stress σ_b versus column length L and wall thickness δ for $f = 0.2$ and 0.8 (for $n = 1 - 5$, $a = 0.3$ m, material models (A) and (B))

on all considered cases, the discrepancies between the analytical and numerical results should not exceed 10% (with the correction factor ψ).

It should be noted that the buckling stresses increase with the fibre volume fraction, similar to the minimum critical stress. Furthermore, the minimum critical stresses are slightly affected by the type of material homogenization method (see Figs. 14, 15). The model (B) [4] case exhibits smaller critical stresses than in the case of model (A) [21], but the difference is not great. It should be noted that, comparing the analytical values calculated for (A) and (B) in Table 3, relative deviations of between 12% and 19% are found. This observation is very important from an engineering (practical) point of view because in the estimation of effective material parameters, uncertainties strongly affect the reliability of buckling analysis. Moreover, the characteristic length depends significantly on the type of material homogenization method. In the case of simple homogenization method (B) [4], the characteristic length is visibly greater than that in the model (A) case [21].

Finally, it should be noted that the numerical results obtained confirm the validity of the theoretical assumptions adopted for the theoretical considerations leading to the analytical solutions.

	(A)			(B)				(A)			(B)		
	$\sigma_{cr,min}$ [MPa]	a [m]	δ [m]	$\sigma_{cr,min}$ [MPa]	a [m]	δ [m]		$\sigma_{cr,min}$ [MPa]	a [m]	δ [m]	$\sigma_{cr,min}$ [MPa]	a [m]	δ [m]
pt	17.74	0.5	0.001	15.21	0.5	0.001	pt	63.87	0.5	0.001	50.99	0.5	0.001

Fig. 13 Minimum critical stresses $\sigma_{cr,min}$ versus cross-sectional height a and wall thickness δ for $f = 0.2$ and 0.8 (for material models (A) and (B))
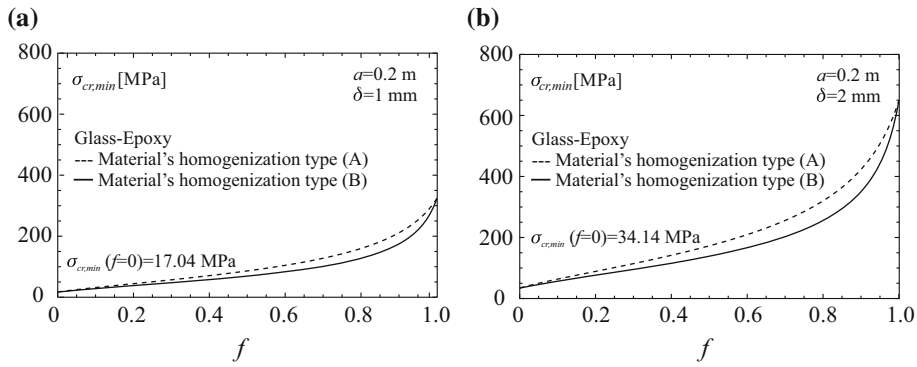
Fig. 14 Minimum critical stresses $\sigma_{cr,min}$ versus fibre volume fraction f for two wall thicknesses and for both material homogenization types (A) and (B) at **a** $\delta = 1$ mm and **b** $\delta = 2$ mm
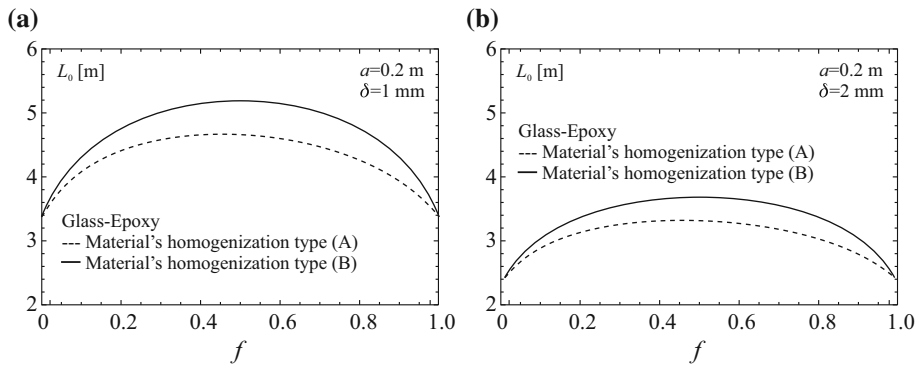
Fig. 15 Characteristic member length L_0 versus fibre volume fraction f for two wall thicknesses and both material homogenization types (A) and (B) at **a** $\delta = 1$ mm and **b** $\delta = 2$ mm
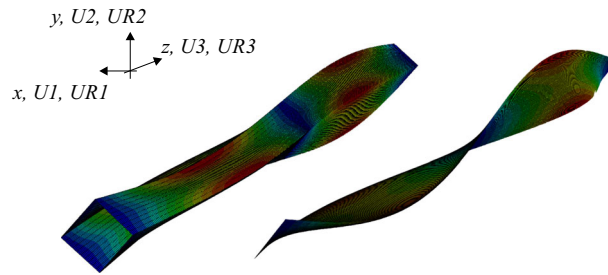
Fig. 16 Buckling modes for a column with one internal diaphragm for the full geometry of the cross section and for a quarter of the cross section based on symmetry ($L = 4$ m, $a = 0.2$ m, $\delta = 0.001$ m)
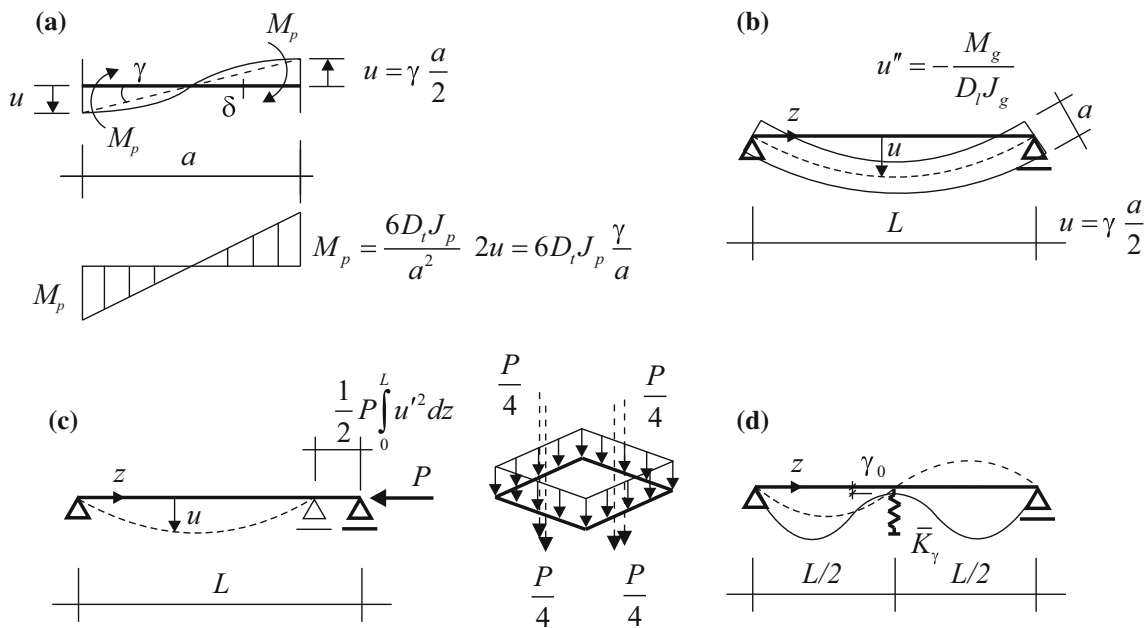
Compliance with ethical standards

Conflict of interest The author declares that he has no conflict of interest.

Appendix A

Fig. 17 Figures complementing the analytical considerations: **a** the bending stiffness of the web in the transverse direction (the case of bending of the column), **b** displacements of the wall subjected to bending, **c** axial end loads and axial displacements of the support, and **d** the influence of diaphragm stiffness on the number of half-waves

References

1. Abambres, M., Camotim, D., Silvestre, N.: GBT-based elastic-plastic post-buckling analysis of stainless steel thin-walled members. Thin Walled Struct. **83**, 85–102 (2014)
2. Abambres, M., Camotim, D., Silvestre, N., Rasmussen, K.: GBT-based structural analysis of elastic-plastic thin-walled members. Comput. Struct. **136**, 1–23 (2014)
3. Ádány, S., Silvestre, N., Schafer, B., Camotim, D.: GBT and cFSM: two modal approaches to the buckling analysis of unbranched thin-walled members. Adv. Steel Constr. **5**(2), 195–223 (2009)
4. Berthelot, J.: Composite Materials—Mechanical Behaviour and Structural Analysis. Springer, Berlin (1999)
5. Camotim, D., Basaglia, C., Silvestre, N.: GBT buckling analysis of thin-walled steel frames: a state-of-the-art report. Thin Walled Struct. **48**, 726–743 (2010)
6. Cheung, Y.: Finite Strip Method in Structural Analysis. Elsevier, Amsterdam (1976)
7. Cheung, Y., Tham, L.: Finite Strip Method. CRC Press, Boca Raton (1998)
8. Chudzikiewicz, A.: Stability loss due to the deformation of the cross-section. Eng. Trans. **7**(1), 45–61 (1960)
9. Daniel, I., Ishai, O.: Engineering Mechanics of Composite Materials. Oxford University Press, Oxford (2006)
10. Davies, J.: Recent research advances in cold-formed steel structures. J. Constr. Steel Res. **55**, 267–288 (2000)
11. Dinis, P., Camotim, D., Silvestre, N.: GBT formulation to analyse the buckling behaviour of thin-walled members with arbitrarily 'branched' open cross-sections. Thin Walled Struct. **44**, 20–38 (2006)
12. Dow, N., Rosen, B.: Evaluation of Filament-reinforced Composites for Aerospace Structural Applications. NASA Contractor Report. General Electric Company, Philadelphia (1965)
13. Eliseev, V., Vetyukov, Y.: Finite deformation of thin-walled shells in the context of analytical mechanics of material surfaces. Acta Mech. **209**(1–2), 43–57 (2010)
14. Gonçalves, R., Camotim, D.: GBT deformation modes for curved thin-walled cross-sections based on a mid-line polygonal approximation. Thin Walled Struct. **103**, 231–243 (2016)
15. Habbit, D., Karlsson, B., Sorensen, P.: ABAQUS Analysis User's Manual. Hibbit, Karlsson, Sorensen Inc, Providence (2007)
16. Hancock, G., Pham, C.: Buckling analysis of thin-walled sections under localised loading using the semi-analytical finite strip method. Thin Walled Struct. **86**, 35–46 (2015)
17. Jones, R.: Mechanics of Composites Materials. Taylor & Francis, Abingdon (1999)
18. Kaw, A.: Mechanics of Composite Materials. Taylor & Francis, Abingdon (2006)
19. Kelly, A. (ed.): Concise Encyclopaedia of Composite Materials. Pergamon Press, Oxford (1989)
20. Kollar, L., Springer, G.: Mechanics of Composite Structures. Cambridge University Press, Cambridge (2003)
21. Królak, M., Mania, R. (eds.): Stability of Thin-Walled Plate Structures. Technical University of Łódź, Łódź (2011)
22. Kujawa, M., Szymczak, C.: Elastic distortional buckling of thin-walled bars of closed quadratic cross-section. Mech. Mech. Eng. **17**(2), 119–126 (2013)
23. Li, Z., Abreu, J., Leng, J., Schafer, B.: Review: constrained finite strip method developments and applications in cold-formed steel design. Thin Walled Struct. **81**, 2–18 (2014)
24. de Miranda, S., Gutiérrez, A., Miletta, R., Ubertini, F.: A generalized beam theory with shear deformation. Thin-Walled Struct. **67**, 88–100 (2013)
25. Philips, L.: Design with Advanced Composite Materials. Springer, Berlin (1989)
26. Pietraszkiewicz, W., Górski, J. (eds.): Shell Structures: Theory and Applications, vol. 3. CRC Press, Boca Raton (2014)
27. Pietraszkiewicz, W., Kreja, I. (eds.): Shell Structures: Theory and Applications, vol. 2. CRC Press, Boca Raton (2010)
28. Pietraszkiewicz, W., Szymczak, C. (eds.): Shell Structures: Theory and Applications, vol. 1. Taylor & Francis, Abingdon (2005)
29. Pietraszkiewicz, W., Witkowski, W. (eds.): Shell Structures: Theory and Applications, vol. 4. CRC Press, Boca Raton (2018)
30. Schardt, R.: Generalized beam theory—an adequate method for coupled stability problems. Thin Walled Struct. **19**, 161–180 (1994)
31. Silvestre, N., Camotim, D.: Second-order generalised beam theory for arbitrary orthotropic materials. Thin Walled Struct. **40**, 791–820 (2002)
32. Szymczak, C., Kujawa, M.: Distortional buckling of thin-walled columns of closed quadratic cross-section. Thin Walled Struct. **113**, 111–121 (2017)
33. Szymczak, C., Kujawa, M.: Local buckling of composite channel columns. Contin. Mech. Thermodyn. (2018). https://doi.org/10.1007/s00,161-018-0674-2
34. Thompson, J., Hunt, G.: A General Theory of Elastic Stability. Wiley, Hoboken (1973)
35. Timoshenko, S., Gere, J.: Theory of Elastic Stability. McGraw-Hill, International Book Company, New York (1961)
36. Vasiliev, V., Morozov, E.: Mechanics and Analysis of Composites Materials. Elsevier, Amsterdam (2001)
37. Vetyukov, Y.: Direct approach to elastic deformations and stability of thin-walled rods of open profile. Acta Mech. **200**, 167–176 (2008)
38. Vetyukov, Y.: Nonlinear Mechanics of Thin-Walled Structures. Springer, Berlin (2014)
39. Waszczyszyn, Z. (ed.): Modern Methods of Stability Analysis of Structures. Ossolineum, Wrocław (1981)
40. Waszczyszyn, Z. (ed.): Selected Problems of Stability of Structures. Ossolineum, Wrocław (1987)
41. Zienkiewicz, O., Taylor, R.: The Finite Element Method, 7th edn. Elsevier, Amsterdam (2013)